RSC Advances

PAPER

View Article Online
View Journal | View Issue

Cite this: *RSC Adv.*, 2021, **11**, 35954

Vertically stacked GaN/WX_2 (X = S, Se, Te) heterostructures for photocatalysts and photoelectronic devices

Dahua Ren, *[ab] Yunhai Li[b] and Wenqi Xiong [b]

Received 30th September 2021
Accepted 1st November 2021

DOI: 10.1039/d1ra07308g

rsc.li/rsc-advances

Tremendous attention has been paid to vertically stacked heterostructures owing to their tunable electronic structures and outstanding optical properties. In this work, we explore the structural, electronic and optical properties of vertically stacked GaN/WX_2 (X = S, Se, Te) heterostructures using density functional theory. We find that these stacking heterostructures are all semiconductors with direct band gaps of 1.473 eV (GaN/WTe_2), 2.102 eV (GaN/WSe_2) and 1.993 eV (GaN/WS_2). Interestingly, the GaN/WS_2 heterostructure exhibits a type-II band alignment, while the other two stackings of GaN/WSe_2 and GaN/WTe_2 heterostructures have type-I band alignment. The optical absorption of GaN/WX_2 heterostructures is very efficient in the visible light spectrum. Our results suggest that GaN/WX_2 heterostructures are promising candidates for photocatalytic water splitting and photoelectronic devices in visible light.

Introduction

Van der Waals (vdW) heterostructures (HS) are used to design unusual electronic devices because of their peculiar physical properties and immense performances.[1] Additionally, vertically stacked heterostructures have innovative applications in electronic devices, such as ultrathin photodetectors,[2] solar cells,[3] memory devices,[4] flexible sensors and transistors[5,6] *etc.* Specifically, two-dimensional (2D) vdW heterostructures with type-II band alignments have promising potential in photovoltaics devices and photocatalysts[7–11] due to their fascinating electronic and optical properties. In type-II heterostructures, the photogenerated holes and electrons become spatially located in different layers. As a result, the recombination of carriers can be effectively prevented and the light energy utilization is significantly enhanced.[12] Moreover, 2D WX_2 (X = S, Se, Te) is a typical layered transition metal dichalcogenide family, which has a direct band gap from 1.0 eV to 2.4 eV.[13–22] Among the transition metal dichalcogenides (TMD) materials, monolayer WS_2, WSe_2, and 1H WTe_2 are typically semiconductors with direct band gaps of 2.38 eV,[18,19] 2.11 eV,[20,21] 1.46 eV.[22]

Motivated by 2D graphene-like planar honeycomb structures, 2D group III–V compound semiconductors with planar hexagonal structures have been predicted to be stable.[23–26] In particular, the monolayer hexagonal structure of gallium nitride (GaN) has recently received growing attractions, which has been directly experimentally synthesized *via* graphene encapsulation.[25] Onen *et al.* reported that the indirect band gap of 2D GaN is 3.42 eV with HSE06 calculation,[26] but the indirect bandgap hindered the practical applications in optoelectronics. In addition, heterostructures based on 2D GaN, such as GaN/blueP, GaN/MoS_2, GaN/$MoSe_2$, GaN/WS_2, $MoSe_2$/blueP, GaN/ZnO and GaN/BP heterostructures, are able to be formed to type-II band structures, which show good electronic and optical behaviors in photocatalyst and optoelectronic applications.[27–32]

It is also worth to note that 2D WX_2, together with 2D GaN, can form vdW heterostructures for their similar structures and same lattice constants. Generally, the superior structures and excellent properties of GaN/WX_2 (X = S, Se, Te) heterostructures are significantly valuable to explore, which could potentially provide a platform for applications in photocatalyst and optoelectronic devices.

Computational methods

Ab initio calculations were performed within the framework of density functional theory (DFT),[33,34] as implemented in the Vienna *Ab Initio* Simulations Package (VASP).[35] Electronic exchange and correlation effects were described with the Perdew–Burke–Ernzerhof (PBE)[36] functional of generalized gradient approximation (GGA)[37] and HSE06 hybrid function.[38] Electron–ion interaction were treated with the projector augmented wave (PAW) method,[39,40] with an energy cutoff of 550 eV. And Brillouin zone sampling of *K*-mesh was set to 9 × 9 × 1 for relaxation. Subsequently, *K*-mesh points for density of states (DOS) and energy band structures were set to 13 × 13 × 1 and the energy criteria were set as 10^{-5} eV until the residual force was smaller than 10^{-3} eV $Å^{-1}$. Especially, the vacuum layer thickness was set more than 25 Å to avoid spurious interactions in the neighboring images. As the long-range vdW interaction is

[a]*School of Information Engineering, Hubei Minzu University, Enshi, 44500, China. E-mail: rdh_perfect@163.com*

[b]*Science of Physics and Technology, Wuhan University, Wuhan, 430072, China*

important to hold the 2D heterostructure together, the vdW-D3 approach[41] was used to describe long-range electron correlation effects.

The optical properties of 2D GaN/WX_2 heterostructures are described by the complex dielectric function $\varepsilon(\omega) = \varepsilon_1(\omega) + i\varepsilon_2(\omega)$, where $\varepsilon_1(\omega)$ and $\varepsilon_2(\omega)$ are real and imaginary parts, respectively. At the same time, the imaginary part is calculated by summing up all possible transitions from the occupied to unoccupied states, which is closely related to the band structure in the absorption behaviors.[42] The imaginary part is given by:

$$\varepsilon_2(\hbar\omega) = \left(\frac{4\pi^2 e^2}{m\omega^2}\right)\sum_{i,j}\int_k \langle i|M|j\rangle^2 f_i\left(1 - f_i^i\right) \times \delta\left(E_{j,k} - E_{i,k} - \omega\right)d^3k \quad (1)$$

where e, m and ω are the charge, mass of free electrons, and the frequency of incident photons, respectively. Meanwhile, M, i, j and f_i are the dipole momentum, indices of initial and final states, and the Fermi–Dirac distribution function for ith state with wave vector $\mathbf{k}$, respectively. The real part $\varepsilon_1(\omega)$ is obtained from the imaginary $\varepsilon_2(\omega)$ by Kramers–Kronig relation:[43,44]

$$\varepsilon_1(\omega) = 1 + \frac{2}{\pi}P\int_0^\infty \frac{\omega'\varepsilon_2(\omega')\mathrm{d}\omega'}{\left(\omega'^2 - \omega^2\right)} \quad (2)$$

where P is the principal value. Absorption coefficient is then obtained as:[43,44]

$$\alpha(\omega) = \frac{\sqrt{2}\omega}{c}\left[\sqrt{\varepsilon_1{}^2(\omega) + \varepsilon_2{}^2(\omega)} - \omega_1(\omega)\right]^{1/2} \quad (3)$$

Results and discussion

Stability and structures

Stacking patterns can modulate the electronic properties of the vdW heterostructures. Therefore, four typical stacking configurations (AA, AB, AC, AD) have been constructed. In the AA stacking, the Ga atom sits on the top of S/Se/Te atom, while the N atom is on top of W atom. In the AB stacking, the Ga atom is placed on the top of W atom, while the N atom is on the center of the hexagonal site. In the AC stacking, the N atom sits on the top of W atom, while the Ga atom is located on the center of the hexagonal site. In the AD stacking, the Ga atom sits on the top of W atom, while the N atom is on top of S/Se/Te atom. These relaxed structures are shown in Fig. 1. For GaN/WS_2 heterostructure, the interface binding energies of AA, AB, AC and AD stacking patterns are −27.72 meV Å^{-2}, −27.01 meV Å^{-2}, −26.69 meV Å^{-2}, and −22.58 meV Å^{-2} respectively. In consistence with other reports,[27,28] after relaxation, AA stacking of GaN/WX_2 heterostructures are the most stable due to the lowest interface binding energies. AA stacking patterns are only taken into consideration in the next calculation. The equilibrium lattice constants $a(b)$, bond lengths, bond angles of GaN monolayer, WX_2 monolayer and AA stacking GaN/WX_2 heterostructures, calculated with GGA–PBE, are listed in Table 1. From Table 1, the calculated lattice constants, bond lengths/angles accord well with previous reports.[13,14,16,23,24,26,28] And the relaxed crystal structures of the GaN, WS_2, WSe_2, and WTe_2 monolayers and GaN/WX_2 bilayers are hexagonal. It is clear that the hexagonal unit parameters of GaN/WS_2, GaN/WSe_2, GaN/WTe_2 heterostructures are 3.194 Å, 3.285 Å, 3.388 Å, respectively, which agree well with previous results.[28,29] The lattice mismatches are expressed as $\omega = \frac{|a-c|}{a} \times 100\%$. Where a and c are lattice constants of GaN/WX_2 heterostructure and individual WX_2 layer or GaN layer. The lattice mismatches of GaN/WS_2, GaN/WSe_2, GaN/WTe_2 heterostructures are 1.7%, 3.0% and 3.4%, meaning that the differences are negligible.

To describe the vdW interactions, the interface binding energies (ΔE) of GaN/WX_2 heterostructures are calculated as:

$$\Delta E = (E_{HS} - E_{GaN} - E_{WX_2})/S_0 \quad (4)$$

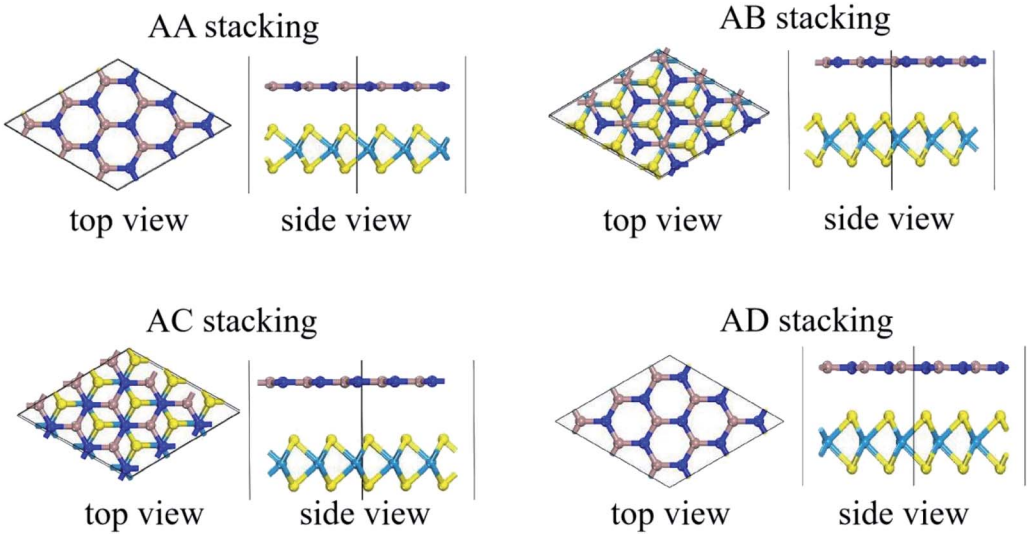

Fig. 1 Relaxed structures of four typical stacking patterns of GaN/WX_2 (X = S, Se, Te) heterostructures. Cyan, yellow, dark blue, and brown spheres indicate W, X, N and Ga atoms, respectively.

Table 1 Lattice parameters $a(b)$, bond lengths $l_{X-W}(l_{Ga-N})$, bond angles Θ_{XWX}, interface equilibrium distances d_{eq} and the interface binding energies ΔE were calculated using PBE in comparison to previous theoretical and experimental values

Name		a (b)/Å	l_{X-W}/Å	l_{Ga-N}/Å	Θ_{XWX}/°	d_{eq}/Å	ΔE/meV·Å^{-2}
GaN	Theo.	3.21[a], 3.25[b]		1.85[a]	—	—	—
	Cal.	3.248	—	1.858	—	—	—
	Expt.	3.20[c]			—	—	—
WS_2	Theo.	3.18[d], 3.14[f]	2.42[d]		81.01[d]	—	—
	Cal.	3.185	2.411	—	81.023	—	—
	Expt.	3.155[e]				—	—
WSe_2	Theo.	3.32[d], 3.31[g]	2.55[d]		82.43[d]	—	—
	Cal.	3.295	2.517	—	82.749	—	—
	Expt.	3.286[e]			—	—	—
WTe_2	Theo.	3.51[g]			—	—	—
	Cal.	3.502	2.736	—	83.334	—	—
GaN/WS_2	Theo.	3.200[f]	2.433[f]	1.852[h]	—	3.479[f]	−33.36[f], −19.61[h]
	Cal.	3.194	2.431	1.845	81.144	3.081	−27.72
GaN/WSe_2	Theo.	3.29[h]	—	—	—	—	−21.87[h]
	Cal.	3.285	2.543	1.897	82.417	3.139	−28.05
GaN/WTe_2	Cal.	3.388	2.810	1.906	83.799	3.236	−37.63

[a] Ref. [26]. [b] Ref. 23. [c] Ref. 25. [d] Ref. 16. [e] Ref. 14. [f] Ref. 28. [g] Ref. 13. [h] Ref. 29.

where ΔE refers to the interface binding energies at the interface of GaN/WX_2 heterostructures, and E_{HS}, E_{GaN}, E_{WX_2}, S_0 represent the total energies of heterostructures, GaN monolayer, WX_2 monolayer, the interface areas of the heterostructures, respectively. The interface areas of the heterostructures are calculated by multiplying $\boldsymbol{a}$ and $\boldsymbol{b}$ vectors in hexagonal unit cells. Then, the interface binding energies of GaN/WX_2 heterostructures are listed in Table 1, consistent with other theoretical reports.[28,29] As is shown in Fig. 2, the optimal distances between N atom in the GaN layer and X atom in the WX_2 layer are 3.081 Å, 3.139 Å, 3.236 Å, respectively, indicating that no bonds between Ga and X atoms are formed and all these heterostructures are formed by the same magnitude order of van der Waals (vdW) forces as others, such as GaN–blueP,[27] GaN/WS_2,[28] GaN/BP[30] and typical vdW graphite.[45]

Obviously, the interface binding energies of GaN/WS_2, GaN/WSe_2 and GaN/WTe_2 heterostructures are −27.72, −28.05, and −37.63 meV Å^{-2}, demonstrating that the interactions between two layers belong to physically vdW forces. All the interface binding energies are negative, suggesting that the GaN/WX_2 heterostructures have favorable energies during the formation.

Electronic properties

In the following section, projection-resolved band structures of GaN/WX_2 heterostructures are depicted in Fig. 3. All the GaN/WX_2 heterostructures are direct band gap semiconductors. Both the valence band maximum (VBM) and the conduction band minimum (CBM) of the GaN/WX_2 (X = S, Se, Te) heterostructures locate at the K point of Brillouin zone (BZ). The band gaps of GaN/WS_2, GaN/WSe_2, GaN/WTe_2 heterostructures are 1.993 eV, 2.102 eV, 1.473 eV, smaller than both individual GaN (3.241 eV) layer and individual WS_2 (2.357 eV), WSe_2 (2.119 eV), WTe_2 (1.594 eV) layer according to HSE06 calculations, which agrees well with the theoretical values of GaN (3.23 eV),[23] WTe_2 (1.49 eV)[22] and experimental values of WS_2 (2.38 eV),[5] WSe_2 (2.11 eV).[8] Specially, GaN/WS_2 heterostructure has a type II band alignment, which is beneficial to the separation of the photogenerated holes and electrons in different layers, the prevention of the recombination of carriers, and the enhancement of the light energy utilization. It is also found that the GaN/WSe_2 and GaN/WTe_2 heterostructures have type-I band alignment semiconductors for both the VBM and CBM of GaN/WSe_2 and GaN/WTe_2 heterostructures come from the W-dz^2 orbitals of the WSe_2 and WTe_2 layer, which can be used in light emitting diodes (LED),[46] indicating that the interlayer interactions between the GaN layer and the WX_2 (X = Se, Te) layer reduce the band gap values. Therefore, the band gaps of the GaN/WX_2 heterostructures could be significantly changed by vertically stacked heterostructures, which could provide a good opportunity to work on band engineering and electronic device

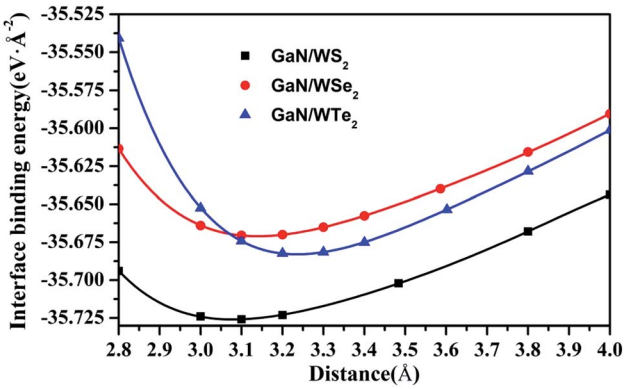

Fig. 2 Plot of interface binding energies as function of interlayer distances for GaN/WS_2, GaN/WSe_2, and GaN/WTe_2 heterostructures. 5th order polynomial has been employed for fitting. In order to clarify the equilibrium distances between the GaN layer and WX_2 layer, the values of interface binding energies of both the GaN/WSe_2 and GaN/WTe_2 heterostructures are shifted downwards by 1.80 eV, 5.40 eV, respectively.

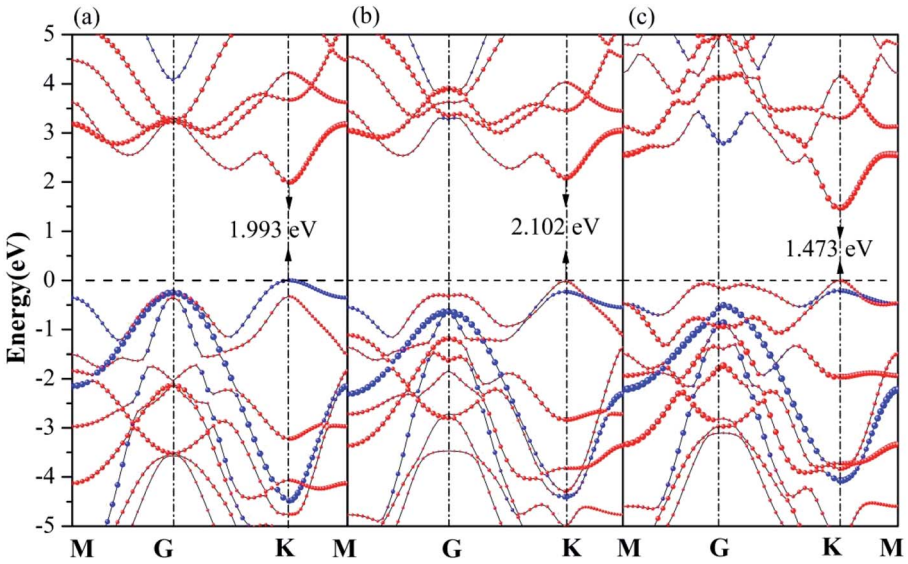

Fig. 3 Projection-resolved band structures of (a) GaN/WS_2, (b) GaN/WSe_2, and (c) GaN/WTe_2 heterostructures. Blue and red lines indicate contributions from GaN and WX_2 layer, respectively.

designs. It is interesting that the band gap of GaN/WS_2 heterostructure is larger than the minimum required energy of the photocatalytic reaction (1.23 eV), which is potential for a photocatalyst in water splitting.

As reflected in the projection-resolved band structures, the band gap of WX_2 monolayer is decreased by the downshift of CBM as well as the upshift of VBM at *K* point. The contribution of VBM of GaN/WS_2 heterostructure is GaN layer and that of CBM is WS_2 layer. In Fig. 4(a), the blue and red lines present the DOS of GaN and WS_2 layer in GaN/WS_2 heterostructure. Both the contributions of VBM and CBM of GaN/WSe_2 and GaN/WTe_2 heterostructures are derived from WSe_2 and WTe_2 layer, as shown in Fig. 4(b and c). Obviously, for GaN/WS_2 heterostructure, the VBM and CBM are respectively confined in GaN and WS_2 layer, which also demonstrates that GaN/WS_2 heterostructure has a type-II band alignment.

Photocatalyst and optoelectronic performances

The absorption coefficients of GaN/WX_2 heterostructures are calculated, as illustrated in Fig. 5(a). It is clear that the first peaks in absorption spectrum of GaN/WS_2, GaN/WSe_2, GaN/WTe_2 heterostructures locate at 3.03, 2.69, 2.25 eV, which are mainly contributed by WX_2 layers. The absorption spectrum of GaN/WX_2 heterostructures covers the whole incident solar spectrum,[47] which makes well suitable applications for optoelectronic devices in visible light.

A schematic plot of migrating carriers to depict the dynamic processes of photogenerated carriers at the GaN/WS_2 interface is shown in Fig. 5(b). In the GaN/WS_2 heterostructure, the photogenerated electrons start to transfer from the GaN layer the WS_2 layer in the conduction band, which is motivated by the conduction band offset (CBO) (0.71 eV). Meanwhile, the

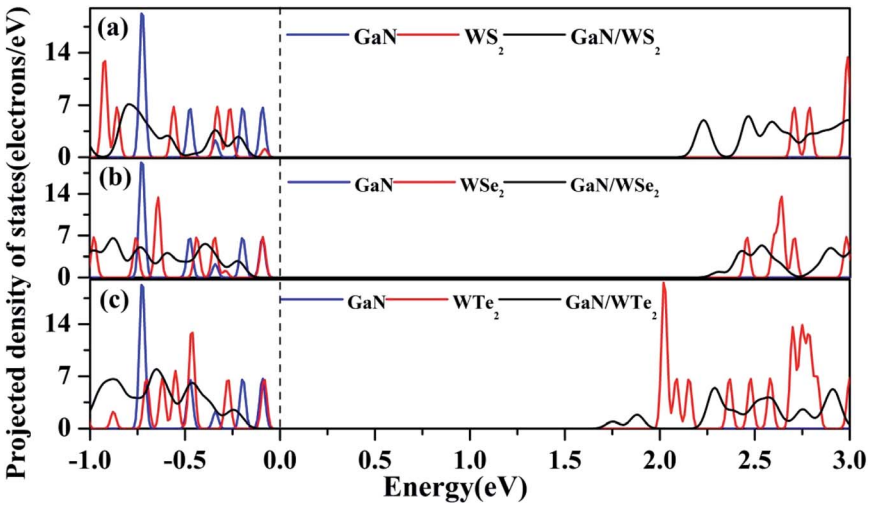

Fig. 4 Projected density of states (PDOS) of (a) GaN/WS_2, (b) GaN/WSe_2, and (c) GaN/WTe_2 heterostructures. Fermi level is set to zero as indicated by the black dashed line.

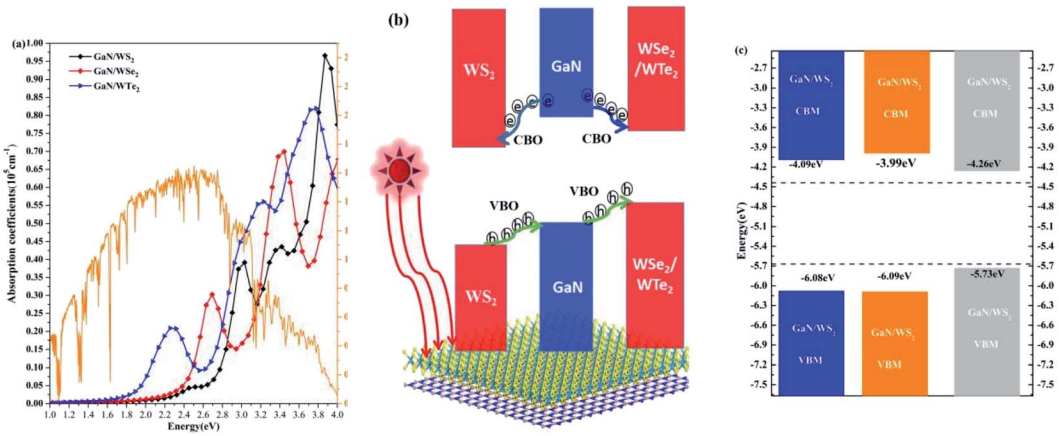

Fig. 5 (a) Absorption spectrum of GaN/WS_2, GaN/WSe_2, and GaN/WTe_2 heterostructures. Incident AM 1.5 G solar flux[48] is plotted in orange solid line. (b) Schematic plot of the migration of photogenerated electrons and holes at the GaN/WS_2 interface. (c) Band-edge alignments of GaN/WX_2 heterostructures.

photogenerated holes in the valence band move from the WS_2 layer to the GaN layer, which are driven by a large valence band offset (VBO) (1.60 eV). Hence, the GaN/WS_2 heterostructure, owing a type-II band alignment, could be utilized as a photocatalyst. As for the GaN/WSe_2 and GaN/WTe_2 heterostructures, one can see that all the photogenerated carriers of the GaN layer are likely to move to the WSe_2 (WTe_2) layer. The VBO and CBO between GaN and WSe_2 (WTe_2) layers are 1.98 eV (2.97 eV) and 0.86 eV (1.72 eV), respectively. As a result, the photogenerated carriers can be located in the WSe_2 (WTe_2) layers to build light-emitting diodes (LEDs).[46] The band edge positions of GaN/WS_2, GaN/WSe_2, GaN/WTe_2 heterostructures are illustrated in Fig. 5(c). The CBMs of GaN/WS_2, GaN/WSe_2, GaN/WTe_2 heterostructures are −4.09, −3.99, −4.26 eV, respectively, whereas the VBMs of GaN/WS_2, GaN/WSe_2, GaN/WTe_2 heterostructures are −6.08, −6.09, −5.73 eV, respectively. Those are within the oxidation potential (E_{O_2/H_2O}, −5.67 eV) of water and the reduction potential (E_{H^+/H_2}, −4.44 eV). Especially, the redox reaction in the GaN/WS_2 heterostructure occurs in different layers: water oxidation occurs in the GaN layer, meanwhile water reduction takes place in the WS_2 layer.

It is well known that the lifetime of photogenerated carriers is significantly influenced by the build-in electric field. Hence, build-in electric field induced by ground state charge transfer were investigated. Based on Bader charge analysis,[48] the charge transfer from the GaN layer to the WS_2 layer is 0.029*e*, leading to an electric field pointing to GaN from WS_2. This electric field will promote the migration of electrons from the GaN layer to WS_2 layer and holes from the WS_2 layer to GaN layer. The build-in electric field $E = P/\varepsilon_0\varepsilon_r S_0 d_{eq}$ of 3.69×10^9 V m^{-1} is acquired in the junction region of GaN/WS_2 heterostructure. Where $P = \Delta q \cdot d_{eq} = 0.089e\cdot$Å is the size of dipole moment, $\varepsilon_0 = 8.850 \times 10^{-12}$ F m^{-1} refers to the permittivity of free space, $\varepsilon_r = 1$ represents the relative dielectric constant, $S_0 = 8.835 \times 10^{-20}$ m^2 is the interfaces area of the WS_2/GaN heterostructure, $d_{eq} = 3.081 \times 10^{-10}$ m denotes the interlayer equivalent distance.

Conclusions

In summary, the electronic and optical properties of GaN/WX_2 heterostructures have been performed within density functional theory. It is found that all the hexagonal GaN/WX_2 heterostructures are stable semiconductors with direct band gaps. Interestingly, among them, the GaN/WS_2 heterostructure has a type-II band alignment, which is beneficial in photocatalysts for water splitting. However, both the GaN/WSe_2 and GaN/WTe_2 heterostructures exhibit type-I band alignment, which can be utilized in LED. In the GaN/WS_2 heterostructure, the charge transport from the GaN layer to the WS_2 layer is 0.029*e*, based on Bader charge analysis, forming a build-in electric field favorable for charge separation. The build-in electric field $E = P/\varepsilon_0\varepsilon_r S_0 d_{eq}$ of 3.69×10^9 V m^{-1} is acquired in the junction region of GaN/WS_2 heterostructure. The absorption behaviors of GaN/WX_2 heterostructures are also performed, and results show that GaN/WX_2 heterostructures are very efficient at absorbing the visible light to expand the application to photocatalyst and photoelectronic devices.

Conflicts of interest

There are no conflicts to declare.

Acknowledgements

This work is supported by the Natural Science Foundation of China with grants no. 1186040026, Incubation Project for High-Level Scientific Research Achievements of Hubei Minzu University with grants no. 4205009 and the Educational Commission of Hubei Province of China with grant no. T201914.

References

1 A. Geim and I. Grigorieva, *Nature*, 2013, **499**, 419–425.
2 M. Massicotte, P. Schmidt, F. Vialla, K. G. Schädler, P. A. Reserbat, K. Watanabe, T. Taniguchi, K. J. Tielrooij and F. H. L. Koppens, *Nat. Nanotechnol.*, 2015, **11**(1), 42–46.

3 C. H. Lee, G. H. Lee, A. M. van der Zande, W. Chen, Y. Li, M. Han, X. Cui, G. Arefe, C. Nuckolls, T. F. Heinz, J. Guo, J. Hone and P. Kim, *Nat. Nanotechnol.*, 2014, **9**(9), 676–681.
4 L. Britnell, R. V. Gorbachev, R. Jalil, B. D. Belle, F. Schedin, A. Mishchenko, T. Georgiou, M. I. Katsnelson, L. Eaves, S. V. Morozov, N. M. R. Peres, J. Leist, A. K. Geim, K. S. Novoselov and L. A. Ponomarenko, *Science*, 2012, **335**(6071), 947–950.
5 H. Wang, H. Yuan, H. S. Sae, Y. Li and Y. Cui, *Chem. Soc. Rev.*, 2015, **44**(9), 2664–2680.
6 N. Lu, H. Guo, L. Li, J. Dai, L. Wang, W. N. Mei, X. Wu and X. C. Zeng, *Nanoscale*, 2014, **6**(5), 2879–2886.
7 Z. Y. Zhu, K. Ren, H. B. Shu, Z. Cui, Z. M. Huang, J. Yu and Y. J. Xu, *Catalyst*, 2021, **11**(8), 991.
8 Y. C. Fan, X. K. Ma, X. B. Liu, J. R. Wang, H. Q. Ai and M. W. Zhao, *J. Phys. Chem. C*, 2018, **122**(49), 27803–27810.
9 J. B. Lou, K. Ren, Z. M. Huang, W. Y. Huo, Z. Y. Zhu and J. Yu, *RSC Adv.*, 2021, **11**(47), 29576–29584.
10 K. Ren, R. X. Zheng, P. Xu, D. Cheng, W. Y. Huo, J. Yu, Z. R. Zhang and Q. Y. Sun, *Nanomaterials*, 2021, **11**(9), 2236.
11 J. Linghu, T. Yang, Y. Luo, M. Yang, J. Zhou, L. Shen and Y. P. Feng, *ACS Appl. Mater. Interfaces*, 2018, **10**(38), 32142–32150.
12 B. Peng, G. Yu, X. Liu, B. Liu, X. Liang, L. Bi, L. Deng, T. C. Sum and K. P. Loh, *2D Mater.*, 2016, **3**(2), 025020.
13 A. Kumara and P. K. Ahluwalia, *Eur. Phys. J. B*, 2012, **85**, 186.
14 W. S. Yun, S. W. Han, S. C. Hong, I. G. Kim and J. D. Lee, *Phys. Rev. B: Condens. Matter Mater. Phys.*, 2012, **85**(3), 033305.
15 H. Shu, Y. Tong and J. Guo, *Phys. Chem. Chem. Phys.*, 2017, **19**(16), 10644–10650.
16 C. H. Chang, *Phys. Rev. B: Condens. Matter Mater. Phys.*, 2013, **88**, 195420.
17 B. J. Wang, X. H. Li, R. Zhao, X. L. Cai, W. Y. Yu, W. B. Li, Z. S. Liu, L. W. Zhang and S. H. Ke, *J. Mater. Chem. A*, 2018, **6**(19), 8923–8929.
18 H. M. Hill, A. F. Rigosi, K. T. Rim, G. W Flynn and T. F. Heinz, *Nano Lett.*, 2016, **16**, 4831–4837.
19 A. F. Rigosi, H. M. Hill, Y. Li, A. Chernikov and T. F. Heinz, *Nano Lett.*, 2015, **15**(8), 5033–5038.
20 S. Y. Gao, L. Yang and C. D. Spataru, *Nano Lett.*, 2017, **17**, 7809–7813.
21 S. Park, N. Mutz, T. Schultz, S. Blumstengel, A. Han, A. Aljarb, L. J. Li, E. J. W. List-Kratochvil, P. Amsalem and N. Koch, *2D Mater.*, 2018, **5**, 025003.
22 V. Wang, Y. Y. Liang, Y. Kawazeo and W. T. Geng, 2018, arXiv:1806.04285.
23 H. L. Zhuang, A. K. Singh and R. G. Hennig, *Phys. Rev. B: Condens. Matter Mater. Phys.*, 2013, **87**(16), 165415.
24 H. B. Shu, X. H. Niu and X. J. Ding, *Appl. Surf. Sci.*, 2019, **479**, 475–481.
25 Z. Y. Al Balushi, K. Wang, R. K. Ghosh, R. A. Vila, S. M. Eichfeld, J. D. Caldwell, X. Qin, Y. C. Lin, P. A. DeSario, G. Stone, S. Subramanian, D. F. Paul, R. M. Wallace, S. Datta, J. M. Redwing and J. A. Robinson, *Nat. Mater.*, 2016, **15**, 1166.
26 A. Onen, D. Kecik, E. Durgun and S. Ciraci, *Phys. Rev. B: Condens. Matter Mater. Phys.*, 2016, **93**, 085431.
27 M. L. Sun, J. P. Chou, J. Yu and W. C. Tang, *Phys. Chem. Chem. Phys.*, 2017, **19**, 17324.
28 H. B. Shu, *Mater. Sci. Eng., B*, 2020, **261**, 114672.
29 Z. Cui, K. Ren, Y. M. Zhao, X. Wang, H. B. Shu, J. Yu, W. C. Tang and M. L. Sun, *Appl. Surf. Sci.*, 2019, **492**, 513–519.
30 H. B. Shu, M. L. Zhao and M. L. Sun, *ACS Appl. Nano Mater.*, 2019, **2**, 6482–6491.
31 H. B. Shu, Y. Yang and M. L. Sun, *Phys. Chem. Chem. Phys.*, 2019, **21**, 15760.
32 H. B. Shu, *Mater. Adv.*, 2020, **1**, 1849.
33 P. Hohenberg and W. Kohn, *Phys. Rev.*, 1964, **136**, B864.
34 B. Y. Tong and L. J. Sham, *Phys. Rev.*, 1966, **144**(1), 1–4.
35 G. Kresse and J. Hafner, *Phys. Rev. B: Condens. Matter Mater. Phys.*, 1993, **47**, 558–561.
36 J. P. Perdew, J. P. Burke and M. Ernzerhof, *Phys. Rev. Lett.*, 1996, **77**, 3865–3868.
37 K. Burke, J. P. Perdew and M. Ernzerhof, *Int. J. Quantum Chem.*, 1997, **61**, 287–293.
38 J. Heyd, G. E. Scuseria and M. Ernzerhof, *J. Chem. Phys.*, 2003, **118**, 8207–8215.
39 G. Kresse and D. Joubert, *Phys. Rev. B: Condens. Matter Mater. Phys.*, 1999, **59**, 1758–1775.
40 P. E. Blöchl, *Phys. Rev. B: Condens. Matter Mater. Phys.*, 1994, **50**, 17953–17979.
41 S. Grimme, J. Antony, S. Ehrlich and H. Krieg, *J. Chem. Phys.*, 2010, **132**, 154104.
42 M. Gajdoš, K. Hummer, G. Kresse, J. Furthmüller and F. Bechstedt, *Phys. Rev. B: Condens. Matter Mater. Phys.*, 2006, **73**, 045112.
43 S. L. Adler, *Phys. Rev.*, 1962, **126**, 413–420.
44 H. Komsa and A. V. Krasheninnikov, *Phys. Rev. B: Condens. Matter Mater. Phys.*, 2013, **88**, 085318.
45 X. Chen, F. Tian, C. Persson, W. Duan and N. X. Chen, *Sci. Rep.*, 2013, **3**, 3046.
46 S. Nakamura, M. Senoh, N. Iwasa and S. I. Nagahama, *Jpn. J. Appl. Phys.*, 1995, **34**, L797.
47 The AM 1.5 G Spectrum was taken from the NREL website: https://Rredc.Nrel.Gov/Solar/Spectra/Am1.5 and integrated with the trapezoid rule.
48 E. Sanville, S. D. Kenny, R. Smith and G. Henkelman, *J. Comput. Chem.*, 2007, **28**, 899–908.